

Droplets of Good Representations: Grokking as a First Order Phase Transition in Two Layer Networks

Noa Rubin* Inbar Seroussi† Zohar Ringel‡

October 9, 2023

ABSTRACT

A key property of deep neural networks (DNNs) is their ability to learn new features during training. This intriguing aspect of deep learning stands out most clearly in recently reported Grokking phenomena. While mainly reflected as a sudden increase in test accuracy, Grokking is also believed to be a beyond lazy-learning/Gaussian Process (GP) phenomenon involving feature learning. Here we apply a recent development in the theory of feature learning, the adaptive kernel approach, to two teacher-student models with cubic-polynomial and modular addition teachers. We provide analytical predictions on feature learning and Grokking properties of these models and demonstrate a mapping between Grokking and the theory of phase transitions. We show that after Grokking, the state of the DNN is analogous to the mixed phase following a first-order phase transition. In this mixed phase, the DNN generates useful internal representations of the teacher that are sharply distinct from those before the transition.

1 INTRODUCTION

Feature learning is a process wherein useful representations are inferred from the data rather than being engineered. The success of deep learning is often attributed to this process. This is reflected, in part, by the performance gap between actual deep neural networks and their infinite-width Gaussian Process (GP) counterparts (Williams, 1996; Novak et al., 2018; Neal, 1996). It is also key to transfer learning applications (Weiss et al., 2016) and interpretability (Zeiler & Fergus, 2014; Chakraborty et al., 2017). Yet despite its importance, there is no consensus on how to measure or let alone classify feature learning effects.

Several recent results began shedding light on this matter. One line of work (adaptive kernel approaches) treats the covariance matrices of activation within each layer (kernels) as the key quantities undergoing feature learning. Feature learning would manifest as a deviation of these kernels from those of a random network and their adaptation to the task at hand. While providing a quantification of feature learning in quite generic settings, the equations governing these latent kernels are quite involved and may host a variety of learning phenomena. One such phenomenon (Seroussi et al., 2023), capable of providing a strong performance boost, is that of Gaussian Feature Learning (GFL) : A gradual process in which the covariance matrices of neuron pre-activations change during training so as to increase their fluctuations along label/target relevant directions. Remarkably, despite this smooth adaptation, the pre-activations' fluctuations, across width and training seeds, remain Gaussian. At the same time, the latent kernel itself develops notable spikes in the target direction, indicating feature learning.

*Hebrew University, Racah Institute of Physics, Jerusalem, 9190401, Israel

†Department of Applied Mathematics, School of Mathematical Sciences, Tel Aviv University, Tel Aviv 69978, Israel

‡Hebrew University, Racah Institute of Physics, Jerusalem, 9190401, Israel

Another phenomenon often associated with feature learning is Grokking. This abrupt phenomenon, first observed in large language models running on simple mathematical tasks, involves fast changes to the test accuracy following a longer period of constant and poor performance (Power et al., 2022). Though usually described as a time-dependent phenomenon, Grokking as a function of other parameters, in particular sample size, has been observed. Several authors provided quantitative explanations in the context of specific toy models wherein one can handcraft or reverse engineer the solution obtained by the network (Gromov, 2023; Nanda et al., 2023) or in suitably tailored perceptron models (Liu et al., 2022; Žunkovič & Ilievski, 2022) where, however, representation learning is tricky to define. Given the aforementioned adaptive kernel approaches to deep learning, as well as the universality of Grokking across different DNNs and hyperparameters, it is natural to look for a more unifying picture of Grokking using a formalism that applies to generic deep networks.

In this work, we study Grokking as an equilibrium (or Bayesian) phenomenon driven by sample size, noise, or network width. Utilizing the aforementioned theoretical advancements, we show that Grokking in large-scale models can be classified and predicted through the theory of phase transitions in physics (Landau & Lifshitz, 2013). Studying two different models, a teacher-student with cubic teacher and modular algebra arithmetic, we show the internal state of the DNN, before Grokking is well described by GFL. In contrast, during Grokking, it is analogous to the mixed phase in the theory of first-order phase transitions, and the statistics of pre-activations are described by a mixture of Gaussian (GMFL). In this GMFL state, the latent kernels associated with the DNNs develop entirely new features that alter their sample complexity compared to standard infinite-width GP limits. After Grokking the weights are successfully represented by the networks. Besides providing a framework to classify feature learning effects, our approach provides analytically tractable and quantitative accurate predictions for the above two models.

Our main results are as follows:

- We establish a concrete mapping between the theory of first-order phase transitions, internal representations of DNNs, and Grokking for two non-linear DNN models each having two tunable layers.
- We identify three phases related to Grokking, one which is smoothly connected to the GP limit and two distinct phases involving different GP mixtures.
- For both our models, we simplify the task of learning high-dimensional representations to solving a non-linear equation involving either two (cubic teacher) or one (modular addition teacher) variables. Moreover, for the latter, we determine the location of the phase transition analytically.
- We flesh out a Grokking-based mechanism that can reduce the sample complexity compared to the GP limit.

Prior works. Phase transitions are ubiquitous in learning theory (e.g. Refs. Gardner & Derrida (1988); Seung et al. (1992); Györgyi (1990)), often in the context of replica-symmetry breaking. Connections between Grokking and phase transition were suggested by Nanda et al. (2023) but as far as analytic predictions go, prior work mainly focused on one trainable layer Žunkovič & Ilievski (2022); Arnaboldi et al. (2023) some suggesting those as an effective theory of representation learning Liu et al. (2022). The formalism of Refs. Arnaboldi et al. (2023); Saad & Solla (1995) can potentially be extended to online Grokking with two trainable layers, but would require reducing the large matrices involved. Phase transitions in representation learning have been studied in the context of bifurcation points in the information bottleneck approach (e.g. Tishby & Zaslavsky (2015)), nonetheless, the connection to deep learning remains qualitative. To the best of our knowledge, we provide a novel first-principals connection between grokking and phase transition *in representation learning*.

2 MODELS

2.1 NON-LINEAR TEACHER MODEL

Our first setting consists of a student Erf-network learning a single index non-linear teacher. The student is trained on a training set of size n , $\mathcal{D} = \{\mathbf{x}_\mu, y(\mathbf{x}_\mu)\}_{\mu=1}^n$ with MSE loss. In the following, bold symbol represents a vector. The input vector is $\mathbf{x}_\mu \in \mathbb{R}^d$ with iid Gaussian entries of variance

1. The target function y , is a scalar linear function of \mathbf{x} , with an orthogonal non-linear correction. Specifically, y is given by-

$$y(\mathbf{x}) = \underbrace{\mathbf{w}^* \cdot \mathbf{x}}_{H_1(\mathbf{w}^* \cdot \mathbf{x})} + \epsilon \underbrace{\left((\mathbf{w}^* \cdot \mathbf{x})^3 - 3|\mathbf{w}^*|^2 \mathbf{w}^* \cdot \mathbf{x} \right)}_{H_3(\mathbf{w}^* \cdot \mathbf{x})}. \quad (1)$$

where H_1, H_3 are the first two odd Hermite polynomials, and $\mathbf{w}^* \in \mathbb{R}^d$ are the teacher weights. For simplicity we take here the norm of the teacher weights to be 1, but this has no qualitative effect on the theory as long as we require $|\mathbf{w}^*| \sim \mathcal{O}(1)$. We consider a fully connected non-linear student network with one hidden layer of width N given by

$$f(\mathbf{x}) = \sum_{i=1}^N a_i \operatorname{erf}(\mathbf{w}_i \cdot \mathbf{x}). \quad (2)$$

where $\mathbf{w}_i \in \mathbb{R}^d$ for $i \in [1, N]$ are the students weights.

2.2 GROKING MODULAR ALGEBRA

Here we consider the setting of Ref. Gromov (2023), where the learning task is addition modulo P where P is prime. The network is trained on the following data set

$$\mathcal{D} = \{\mathbf{x}_{nm}, \mathbf{y}(\mathbf{x}_{nm}) \mid m, n \in \mathbb{Z}_P\} \quad (3)$$

where P is prime, and $\mathbf{x}_{nm} \in \mathbb{R}^{2P}$, is a vector such that it is zero in all its coordinates except in the coordinates n and $P+m$ where it is 1 (a ‘‘two-hot vector’’). The target function $\mathbf{y} \in \mathbb{R}^P$ is given by

$$y_p(\mathbf{x}_{nm}) = \delta_{p, (n+m) \bmod P} - 1/P, \quad (4)$$

where δ is the Kronecker delta and $\bmod P$ denote the modulo operation which returns the remainder from the division by P . For the student model, we consider a two-layer deep neural network with a square activation function, given by

$$f_p(\mathbf{x}_{nm}) = \sum_{i=1}^N a_{pi} (\mathbf{w}_i \cdot \mathbf{x}_{mn})^2 \quad (5)$$

where $\mathbf{w}_c \in \mathbb{R}^{2P}$ for $c \in [1, N]$ are the students weights. For brevity, we denote $y_p(\mathbf{x}_{mn}) = y_{nm}^p$, and $f_p(\mathbf{x}_{nm}) = f_{mn}^p$.

2.3 TRAINING THE MODELS

In both cases, we consider networks that are trained with MSE loss to equilibrium using Langevin dynamics via algorithms such as Durmus & Moulines (2017); Neal et al. (2011). We set the gradient noise level (σ^2) and weight decay such that with no data a_i^2, a_{pc}^2 both average to σ_a^2/N under the equilibrium ensemble of fully trained networks. The input layer weights are required to have a covariance of σ_w^2/d in the teacher-student model with $\sigma_w^2 = \mathcal{O}(1)$ and a covariance of 1 in the modular algebra model. The posterior induced by the above training protocol coincides with that of Bayesian inference with a Gaussian prior on the weights defined by the above covariance and measurement noise σ^2 Naveh et al. (2021).

2.4 DERIVATION OUTLINE

Here, we provide an overview of the main steps of our derivation relevant to both the above models. Our main focus is the posterior distribution of weights in the input layer ($p(\mathbf{w}_i)$) and posterior averaged predictions of the network ($f(\mathbf{x})$). To this end, we first follow the adaptive kernel formalism in Seroussi et al. (2023), specifically the mean-field decoupling between the output layer and the input layer valid within our choice of parameters for $N \gg 1$ and $\sigma_a^2 \ll 1$. The resulting action (defined as $-\log(p(\mathbf{w}_i))$ excluding normalization constants independent of \mathbf{w}_i) governing the input layer of the weights in each neuron is identical, thus we omit the neuron index i . The action for each neuron’s weights is then given by the following implicit equation

$$S[\mathbf{w}] = \frac{|\mathbf{w}|^2}{2\sigma_w^2} - \frac{\sigma_a^2}{2N} \sum_{\mu, \nu} \bar{t}(\mathbf{x}_\mu)^T \bar{t}(\mathbf{x}_\nu) \underbrace{\phi(\mathbf{w} \cdot \mathbf{x}_\mu) \phi(\mathbf{w} \cdot \mathbf{x}_\nu)}_{:= \sigma_a^{-2} \bar{Q}_{\mu\nu}}, \quad (6)$$

where ϕ is the activation function and $\bar{\mathbf{t}}$ is the discrepancy between the training-seed-averaged network output and the target given by

$$\bar{\mathbf{t}}(\mathbf{x}_\mu) = \frac{\mathbf{y}(\mathbf{x}_\mu) - \bar{\mathbf{f}}(\mathbf{x}_\mu)}{\sigma^2}. \quad (7)$$

Notably $\bar{\mathbf{t}}$ is not given but determined by solving the following two mean-field self-consistency equations

$$\bar{\mathbf{f}} = Q [Q + \sigma^2 I_n]^{-1} \mathbf{y} \quad (8)$$

where the kernel Q is defined via

$$Q_{\mu\nu} = \sigma_a^2 \langle \phi(\mathbf{w} \cdot \mathbf{x}_\mu) \phi(\mathbf{w} \cdot \mathbf{x}_\nu) \rangle_{\mathcal{S}[\mathbf{w}]} \quad (9)$$

and $\langle \dots \rangle_{\mathcal{S}[\mathbf{w}]}$ denotes averaging over \mathbf{w} with the probability implied by $\mathcal{S}[\mathbf{w}]$.

Next, we deviate from the approach in Ref. Seroussi et al. (2023). The latter approximates the probability induced by $\mathcal{S}[\mathbf{w}]$ through a variational Gaussian approximation. However, to accommodate potential phase transitions, we need to allow a richer set of probability distributions over the weights, for instance, distributions involving Gaussian mixtures. Conveniently we find that as one scales up d, N, n in an appropriate manner, and following some decoupling arguments, $\mathcal{S}[\mathbf{w}]$ has the form $d\hat{\mathcal{S}}[\mathbf{w}]$ where $d \gg 1$ and $\hat{\mathcal{S}}[\mathbf{w}]$ has $O(1)$ coefficients. This allows us to treat the integration underlying $\langle \dots \rangle_{\mathcal{S}[\mathbf{w}]}$ within a saddle-point approximation.

Similarly to the theory of phase transition in physics Landau & Lifshitz (2013), first-order transitions are marked by the appearance of several distinct saddle points, and can also be understood as bifurcation points in the saddle point equation $\nabla \mathcal{S}[\mathbf{w}] = 0$. We find that the action derived in both models allows for three types of solutions which correspond to the three phases of learning described in the introduction. At first, a single saddle centered around $\mathbf{w} = 0$ exists and weights fluctuate in a Gaussian manner around these minima, as in GFL. In the next phase, the distribution is comprised of a weighted average of this zero-saddle and other $|\mathbf{w}| > 0$ saddles. This marks the beginning of Grokking, since this is an indication that the scale of the weights is being learnt. We name this mixture phase the first Gaussian Mixture Feature Learning phase (GMFL-I). After Grokking, only the saddles with $|\mathbf{w}| > 0$ dominate the average (GMFL-II).

Interestingly, these three ‘‘phases’’ are analogous to those encountered in physical first-order phase transitions, for instance, water-vapour transition. Indeed, as one decreases the volume of the system (analogous to increasing n), the vapour continuously increases its density until at some critical pressure, some areas of vapour start condensing into water (where water is a new saddle in the action of the molecules). However, as this condensation drastically reduces the volume, only small droplets of water may appear to balance the overall pressure at its critical value. As the volume decreases further, this mixture of vapour and water droplets develops more and more droplets until at some point all vapour has turned into water and the pressure starts increasing from its critical value.

The above phenomenology is shared by both models, however, the details of the new saddles that appear, as well as the decoupling scheme between the different components of \mathbf{w} differ between both models. We next turn our attention to these details.

3 RESULTS

3.1 NON-LINEAR TEACHER STUDENT MODEL

Our first step here consists of removing the randomness induced by the specific choice of training set. To this end, we consider taking a large n limit while keeping n/σ^2 fixed. This has several merits. At large, n it is natural to replace summations in Eq. (6) by integrals, which can be evaluated directly. Furthermore, in this limit, one obtains an analytical handle on Gaussian processes regression via the equivalence kernel (EK) approximation Rasmussen & Williams (2005); Cohen et al. (2021). Notably, previous works have found reasonable convergence to this approximation, in similar scenarios to ours, for values as low as $n = 100$ and $\sigma^2 = 0.1$ Cohen et al. (2021).

A key element in the EK approximation is the spectrum of the kernel defined by

$$\int d\mu_z Q(\mathbf{x}, \mathbf{z}) \phi_\lambda(\mathbf{z}) = \lambda \phi_\lambda(\mathbf{x}) \quad (10)$$

where μ_z is the dataset measure, which corresponds here to i.i.d. standard Gaussians. Denoting by g_λ the spectral decomposition of the target function on $\phi_\lambda(\mathbf{x})$, the GPR predictions (Eq. 8) are given by

$$\bar{f}(\mathbf{x}) = \sum_\lambda \frac{\lambda}{\lambda + \sigma^2/n} g_\lambda \phi_\lambda(\mathbf{x}) \quad (11)$$

where $\frac{\lambda}{\lambda + \sigma^2/n}$ are the learnability factors. Notably, n only enters through the combination, n/σ^2 which we treat as the effective amount of data. Hence, we can control the amount of learning in two equivalent ways, by either providing more data points or by reducing the noise.

The resulting limit also enables us to identify the two relevant directions in function space, being $H_1(\mathbf{x})$ and $H_3(\mathbf{x})$. Specifically we argue that at large d the operator $Q(\mathbf{x}, \mathbf{y})$ is block-diagonal within the space spanned by $H_1(\mathbf{x})$ and $H_3(\mathbf{x})$. Since it acts on a target having support only on $H_1(\mathbf{x}), H_3(\mathbf{x})$, this limits $\bar{f}(\mathbf{x})$ to this space and hence also $\bar{t}(\mathbf{x}) = [y(\mathbf{x}) - \bar{f}(\mathbf{x})]/\sigma^2$. Our claim is shown to be self-consistent in App. A namely, that making this assumption results in Q and \bar{t} which obey the same assumption. Operationally, we thus take the ansatz

$$\sigma^2 \bar{t}(\mathbf{x}) = b H_1(\mathbf{x}) + c H_3(\mathbf{x}) \quad (12)$$

where $b, c \in \mathbb{R}$ are some unknown constant coefficients. Later, we derive self-consistent equations determining these constants. Given the above ansatz, we turn to the action in Eq. 6, take the continuum approximation where $\sum_{\mu=1}^n \rightarrow n \int d\mu_y$ and find that the integral appearing in the action can be solved exactly (see A.2), to yield the following continuum action

$$\mathcal{S}[\mathbf{w}] = d \left(\frac{|\mathbf{w}|^2}{2\sigma_w^2} - \frac{2n^2\sigma_a^2}{\pi\sigma^4 dN} \frac{(\mathbf{w} \cdot \mathbf{w}^*)^2}{1 + 2|\mathbf{w}|^2} \left(b - \frac{2c(\mathbf{w} \cdot \mathbf{w}^*)^2}{1 + 2|\mathbf{w}|^2} \right)^2 \right) \quad (13)$$

It can be seen here that multiplying n, σ^2 by the same factor α has no effect on the action, in harmony with the EK approximation. Furthermore, it can be seen that taking out a factor of d , one obtains an action $\hat{\mathcal{S}}$ whose coefficients remain 1 when scaling up n, d and N in a linear manner thus inviting the use of saddle point methods. Nonetheless, the action still combines d coupled modes, hence such a saddle point treatment requires some care.

3.1.1 MEAN-FIELD DECOUPLING BETWEEN INPUT WEIGHTS AND SADDLE POINT

The above action fleshes out the special role played by fluctuations of \mathbf{w} along \mathbf{w}^* . These can in fact be decoupled from fluctuations along other directions in the following manner. Assume for the moment, without loss of generality, that \mathbf{w}^* is the cartesian basis vector $[1, 0, 0 \dots 0]$. We can thus decompose $|\mathbf{w}|^2$ appearing the denominators of the action, as $w_1^2 + \sum_{i=2}^d w_i^2$. Our mean-field decoupling amounts to replacing $\sum_{i=2}^d w_i^2$ by its average under the action one gets from making this replacement. The justification for this decoupling comes from the fact that $\sum_{i=2}^d w_i^2$ is a sum of many identical random variables, and hence one expects this quantity to be self-veraging. The resulting effective action is then

$$\tilde{\mathcal{S}}[\mathbf{w} \cdot \mathbf{w}^*] = d \left(\frac{(\mathbf{w} \cdot \mathbf{w}^*)^2}{2\sigma_w^2} - \frac{2n^2\sigma_a^2}{\pi\sigma^4 dN} \frac{(\mathbf{w} \cdot \mathbf{w}^*)^2}{1 + 2(\sigma_w^2 + (\mathbf{w} \cdot \mathbf{w}^*)^2)} \left(b - \frac{2c(\mathbf{w} \cdot \mathbf{w}^*)^2}{1 + 2(\sigma_w^2 + (\mathbf{w} \cdot \mathbf{w}^*)^2)} \right)^2 \right) \quad (14)$$

Conveniently, due to the appearance of a large factor (d) in front of the action, one can use saddle point methods to study this highly non-linear action. This also reveals the source of potential phase transitions. Indeed at large d , the saddles with the lowest action dominate the weights' probability. A first-order phase transition then amounts to a point where two distinct saddles become degenerate

(in terms of action value). Furthermore, a certain degree of universality is evident from the above action as $n^2, \sigma^{-4}, \sigma_a^{-2}$ and N^{-1} only enter as a product. Hence, for instance, doubling N^{-1} would have the exact same effect as doubling n^2 and if a phase transition is to be observed it could be equivalently driven by any of those.

To proceed with deriving quantitative predictions, we note that our computation of the network has now been reduced to tracking only two unknown variables b, c . We recall that these measure the discrepancy in prediction along H_1 and H_3 respectively. The resulting two coupled non-linear equations amount to computing the four matrix elements of Q under the above action, and deriving b and c from Eq. 11, resulting in an explicit expression for the weights’ distribution. See App. A.3 for further technical details. Our results and comparisons with experiments are given in the next section.

3.1.2 TEACHER-STUDENT EXPERIMENTAL RESULTS

To validate the theoretical model, we trained multiple ensembles of networks with different initialization seeds and compared their weight distributions and outputs to the theoretical solutions. Fixing $N = 700, n = 6000, d = 150, \sigma_w^2 = 0.5, \sigma_a^2 = 8, \epsilon = -0.3$, the noise (σ^2), which can also be seen as controlling the effecting amount of data (n_{eff}) was used to drive the transition. Fig. (1) shows the weights’ negative log-probability demonstrating a good agreement with theory, modulo expected finite- d, N, n effects. Increasing the effective amount of data by decreasing σ^2 , initially only changes the Gaussian fluctuations of the weights along the teacher direction but leaves the system within the GFL phase. By lowering σ^2 further, new distinct saddle points appear and become more probable, thereby marking the beginning of the mixed Gaussian phase, GMFL-I. We define the transition to this phase as the point at which the new saddle reaches a non-negligible value defined here as $1/d$ (solid black line). Notably, as d increases and the saddle point becomes exact, any choice of factor will yield the same value of the critical σ^2 . Note that from the point of transition to the GMFL-I scale the theoretical models are no longer accurate, since after this point the network succeeds in generalizing, and thus the assumption that higher-order Hermite polynomials are irrelevant becomes inadequate.

We further note that due to our choice of activation function, weights acquire a reflection symmetry. Hence the above is actually a first-order symmetry-breaking transition. Breaking this symmetry, by adding say a weak bias, would make one of the new saddles more favourable.

Turning to the outputs of the network, Fig. 2 shows the overlap of the network’s output with the linear (left) and cubic (right) teacher components, as a function of both σ^2 and ϵ . The dashed line on the left plot marks the target value for this overlap whereas the solid black line marks the phase transition point using the aforementioned definition. Modulo expected finite-size effects, these ϵ values also mark a transition into a region where cubic features begin to be learnable as evident from the right panel.

The above experiment also points to some potentially powerful complexity aspects of feature learning. Notably, an FCN NNGP kernel induces a uniform prior over cubic polynomials (i.e. all $l = 3$ hyper-spherical harmonics). As there are $n = O(d^3/6!)$ of those it requires $n = 0.5e + 6$ datapoints to learn such target components in our setting (see also Ref. Cohen et al. (2019)). Here this occurs two orders of magnitudes earlier ($n = 6000$). This occurs because the complex prior induced by a *finite* DNN learns the features from the readily accessible linear components of the target and applies them to the non-linear ones. Proving that such “assisted learning” of complex features changes the sample complexity compared to NNGPs requires further work. In App. A.1 we provide an analytical argument in support of this.

3.2 MODULAR ALGEBRA THEORY

3.2.1 DATA-AVERAGED ACTION AND SYMMETRIES

Our first step in treating this model is again to remove the noise coming from the specific choice of training set. To this end, we take the training set to be the entire dataset but control the *effective* amount of data through σ^2 . This can also be viewed as a discrete version of the equivalence kernel

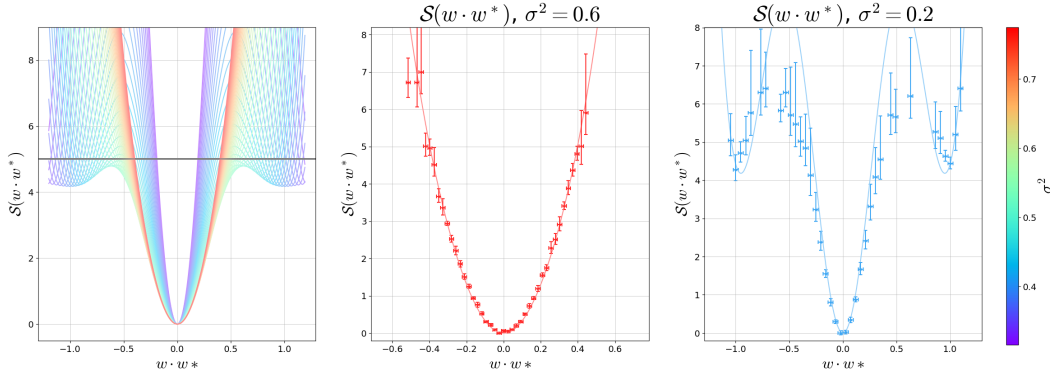


Figure 1: **GFL to GMFL-I Theory and Experiment** Changes in the action (i.e. negative log weight probability along the teacher direction) induced by varying the noise σ^2 . An ensemble of networks was trained for each of the values of epsilon using the method described in C Here $n = 6000$, $\epsilon = -0.3$, $N = 700$, $\sigma_a^2 = 8/N$. Here the transition from the GFL (red) to the GMFL-I (blue) can be observed, with a good match between theory and experiment.

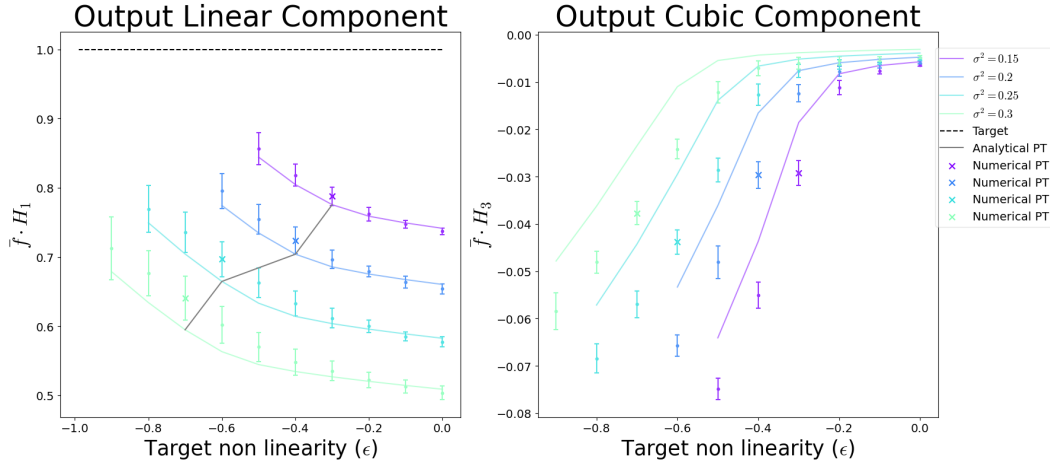


Figure 2: **Average Network Output** Here the linear and cubic components of the average network output can be seen as a function of σ^2, ϵ . The transition to the GMFL-I phase is shown both for the numerical and analytical computation which both agree. The theory successfully predicts the experimental results up to the point of the phase transition, at which point a change in the nonlinear point becomes evident.

approximation Cohen et al. (2019). The resulting action for the input layer weights is then

$$\mathcal{S}[\mathbf{w}] = \frac{|\mathbf{w}|^2}{2} - \frac{\sigma_a^2}{2N} \sum_{p,m,n,m',n'} \bar{t}_{mn}^p \bar{t}_{m'n'}^p (\mathbf{w} \cdot \mathbf{x}_{mn})^2 (\mathbf{w} \cdot \mathbf{x}_{m'n'})^2 + \Gamma[\mathbf{w}] \quad (15)$$

where we added an additional weight decay term $\Gamma[\mathbf{w}]$ which we will soon specify. Evidently, due to the sign of the quartic term, Γ is required to keep the probability normalizable. We will therefore choose a higher-order degree polynomial. This will prevent an explosion of the weights, as is also suggested in Millidge (2022).

An advantage of working with the above action is that all the symmetries of the task are manifested in the action. As we next establish, these symmetries would enable us to reduce the dependence of the action on the high-dimensional vector \bar{t}_{nm}^p to a dependence on a single variable (a) amounting to the overlap of \bar{t}_{nm}^p with the target y_{nm}^p . To this end, we note the following symmetries

- I. Taking $[n, m] \rightarrow [(n + q) \bmod P, (m + q') \bmod P]$, and $f_p \rightarrow f_{(p+q+q') \bmod P}$ with $q, q' \in \mathbb{Z}_P$

II. Taking $[n, m] \rightarrow [qn \bmod P, qm \bmod P]$ and $f_p \rightarrow f_{qp \bmod P}$ for $q \in \mathbb{Z}_P$ but different than zero.

Several outcomes of these symmetries are shown in App. (B.1). First, we find that Q (Eq. 19) is diagonal in the following basis

$$\phi_{k,k'}(x_{n,m}) = P^{-1} e^{2\pi i(kn+k'm)/P} \quad (16)$$

where $k, k' \in \{0, 1, \dots, P-1\}$. Considering eigenvalues, the second symmetry implies that $\phi_{k,k'}$ would be degenerate with $\phi_{ck,ck'}$. For prime, P this implies, in particular, that all $\phi_{k,k}$ eigenvectors with $k > 0$ have the same eigenvalue (λ). Notably, the target itself is spanned by this degenerate subspace specifically

$$y_{nm}^p = P^{-1} \sum_{k=1}^{P-1} e^{-i2\pi kp/P} e^{i2\pi k(n+m)/P} = \left[\sum_{k=1}^{P-1} e^{-i2\pi kp/P} \phi_{k,k}(x_{n,m}) \right] \quad (17)$$

As a result, one finds that the target is always an eigenvector of the kernel and $\bar{t}_{mn}^p = ay_{nm}^p$ where $a = -\frac{\sigma^2}{\lambda + \sigma^2}$. Performing this replacement in Eq. (15) we arrive at our data-averaged action.

3.2.2 DECOUPLING OF WEIGHT MODES

Next, we wish to decouple all the different fluctuating m modes by utilizing again the symmetries of the problem and making a judicial choice of the non-linear weight decay term (Γ). To this end, we define the following Fourier transformed weight variables (w_k, v_k)

$$w_n = \sum_{k=0}^{P-1} w_k e^{-\frac{2\pi i kn}{P}}, \quad v_m = \sum_{k=0}^{P-1} v_k e^{-\frac{2\pi i km}{P}} \quad (18)$$

which when placed into action yields

$$\mathcal{S}[\hat{w}] = P \left[\left(\frac{1}{2} \sum_{k=0}^{P-1} w_k w_{-k} + \frac{1}{2} \sum_{k=0}^{P-1} v_k v_{-k} \right) - \frac{2\sigma_a^2 a^2 P^2}{N} \sum_{k=1}^{P-1} w_k w_{-k} v_k v_{-k} \right] + \Gamma[\mathbf{w}] \quad (19)$$

(see App. B.2) where apart from the non-linear weight-decay term, all different k modes have been decoupled. For simplicity, we next choose, $\Gamma[\mathbf{w}] = \sum_k P \frac{\gamma}{6} \left((w_k w_{-k})^3 + (v_k v_{-k})^3 \right)$.

Following the presence of a large factor of P in front of the action, the above non-linear action, per k -mode, can be analyzed using standard saddle point treatment. Namely, Q as function of a , and with it λ , can be evaluated through a saddle-point approximate on the probability associated with this action. Following this a can be calculated using the GPR expression $-\frac{\sigma^2}{\lambda + \sigma^2}$. Demanding this latter value of a matches the one in the action results in an equation for a .

Conveniently, at any point prior to the phase transition, the resulting equation for a is trivial. Indeed as the quadratic term is constant in the scaled action, as long as no other saddles become degenerate (in action value) with the $|w| = 0$ saddle, the saddle-point treatment truncates the action at this first term. In this region, a stays constant at its infinite width value. Decreasing σ^2 then has the sole effect of making the quartic term more negative. Hence a first-order symmetry-breaking transition must occur at some critical value of σ^2 . Past this point, a begins to diminish. Notably a measures the test-RMSE here. Hence the fact that it remains constant and suddenly begins to diminish can also be understood as Grokking.

Solving the implied equation for a numerically yields the full phase diagram here (see App. B.3 for technical details). Fig. (3) plots the negative-log-probability of weights for an arbitrary k taking $w_k = v_k = w$ for simplicity. Staring at large σ^2 (and solving for $a(\sigma^2)$ numerically), the $|w| \neq 0$ saddles are exponentially suppressed in P , yet nonetheless become more probable as σ^2 decreases. At around $\sigma^2 = 0.227$ they come within $\mathcal{O}(1)$ of the saddle at $S_k(w=0, v=0)$ ($\mathcal{O}(1/P)$ in the plot, given the scaled y-axis). This marks the beginning of the mixed phase (GMFL-I), wherein all action minima contribute in a non-negligible manner. Further, in this phase decreasing σ^2 does not change the height of the $|w| \neq 0$ minima (see inset) in any appreciable manner. Had we zoomed in further, we would see a very minor change to these saddle's height throughout the mixed phase,

as they go from being $O(1)$ above the $|w| = 0$ saddle to $O(1)$ below that saddle at $\sigma^2 \approx 0.175$, as shown in the inset graph in Fig. (3). This latter point marks the beginning of the GMFL-II phase, where it is the contribution of the minimum at $|w| = 0$ which becomes exponentially suppressed in P . Notably a , which measures here the test-RSME, goes from -1 at the beginning of GMFL-I to -0.7 at its end. Over this small interval of σ^2 we observe a 30% reduction in the magnitude of the discrepancy which can be thought of as a manifestation of Grokking.

We comment analyzing more natural weight decay terms such as $\sum_n w_n^6 + w_m^6$, using a certain GP mixture ansatz of $p(w_i)$ as an approximation, we obtained similar qualitative results namely that a GMFL phase is preferable to the GFL phase at low enough N .

Our analytical results are consistent with the experiments carried out in Ref. Gromov (2023). Indeed as we enter GMFL-I, weights sampled near the $|w_k|, |v_k| \neq 0$ saddle, correspond to the cosine expressions for $W_k^{(1)}$ of that work. As our formalism marginalizes over readout layer weights, the phase constraint suggested in their Eq. (12) becomes irrelevant and both viewpoints retrieve the freedom of choosing cosine phases. In our case, this stems from the $U(1) \times U(1)$ complex-phase freedom in our choice of saddles at $|w_k|, |v_k| > 0$

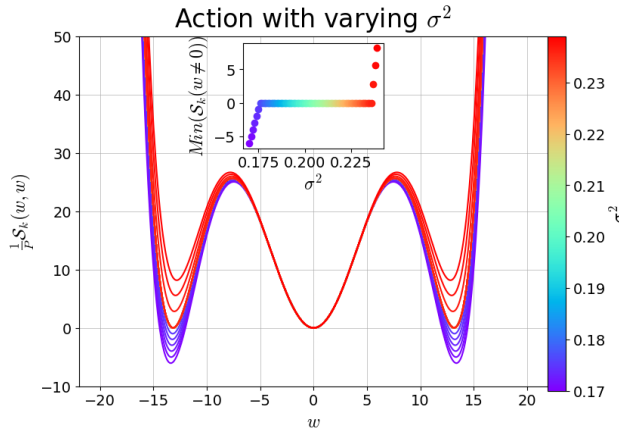


Figure 3: **GFL to GMFL-I to GMFL-II** Probability distribution of weights as predicted by our approach. The GFL phase is represented by the red graphs, where the minimum of the action at zero (shared also by the GP limit) dominates the probability distribution. The GMFL-I phase can be seen in the inset graph, and the final GMFL-II phase is shown in purple. The Parameters taken in this calculation are: $N = 1000$, $P = 401$, $\sigma_a^2 = 0.002/N$, $\gamma = 0.0001$

4 DISCUSSION

In this work, we studied two different models exhibiting forms of Grokking and representation/feature learning. Focusing on equilibrium aspects of Grokking, we extended the approach of Seroussi et al. (2023) to include mixtures of Gaussian. The resulting framework led to concrete analytical predictions for rich feature learning effects exposing, in particular, several phases of learning (GFL, GMFL-I, GMFL-II) in the thermodynamic/large-scale limit. Our results also suggest that feature learning in finite FCNs with mean-field scaling can change the sample complexity compared to the associated NNGP. Certainly, these describe very different behavior compared to the recently explored kernel-scaling Li & Sompolinsky (2021); Ariosto et al. (2022) approach, wherein feature learning amounts to a multiplicative factor in front of the kernel. A potential source of difference here is their use of standard scaling, however, this remains to be explored.

As our results utilize a rather general formalism Seroussi et al. (2023), we believe they generalize to deep networks and varying architecture. As such, they invite further examination of feature learning in the wild from the prism of the latent kernel adaptation. Such efforts may provide, for instance, potential measures of when a model is close to Grokking by tracking outliers in the weight or pre-activation distributions along dominant kernel eigenvectors. As latent kernels essentially provide a spectral decomposition of neuron variance, they may help place empirical observations on

neuron sensitivity and interpretability Zeiler & Fergus (2014) on firmer analytical grounds. Finally, they suggest novel ways of pruning and regulating networks by removing low-lying latent kernel eigenvalues from internal representations.

REFERENCES

- S Ariosto, R Pacelli, M Pastore, F Ginelli, M Gherardi, and P Rotondo. Statistical mechanics of deep learning beyond the infinite-width limit. *arXiv preprint arXiv:2209.04882*, 2022.
- Luca Arnaboldi, Ludovic Stephan, Florent Krzakala, and Bruno Loureiro. From high-dimensional & mean-field dynamics to dimensionless ODEs: A unifying approach to SGD in two-layers networks. *arXiv e-prints*, art. arXiv:2302.05882, February 2023. doi: 10.48550/arXiv.2302.05882.
- Blake Bordelon and Cengiz Pehlevan. Self-consistent dynamical field theory of kernel evolution in wide neural networks. *Advances in Neural Information Processing Systems*, 35:32240–32256, 2022.
- Supriyo Chakraborty, Richard Tomsett, Ramya Raghavendra, Daniel Harborne, Moustafa Alzantot, Federico Cerutti, Mani Srivastava, Alun Preece, Simon Julier, Raghuvver M. Rao, Troy D. Kelley, Dave Braines, Murat Sensoy, Christopher J. Willis, and Prudhvi Gurram. Interpretability of deep learning models: A survey of results. In *2017 IEEE SmartWorld, Ubiquitous Intelligence & Computing, Advanced & Trusted Computed, Scalable Computing & Communications, Cloud & Big Data Computing, Internet of People and Smart City Innovation (Smart-World/SCALCOM/UIC/ATC/CBDCOM/IOP/SCI)*, pp. 1–6, 2017. doi: 10.1109/UIC-ATC.2017.8397411.
- Omry Cohen, Or Malka, and Zohar Ringel. Learning Curves for Deep Neural Networks: A Gaussian Field Theory Perspective. *arXiv e-prints*, art. arXiv:1906.05301, Jun 2019.
- Omry Cohen, Or Malka, and Zohar Ringel. Learning curves for overparametrized deep neural networks: A field theory perspective. *Physical Review Research*, 3(2):023034, 2021.
- Alain Durmus and Eric Moulines. Nonasymptotic convergence analysis for the unadjusted langevin algorithm. *The Annals of Applied Probability*, 27(3):1551–1587, 2017.
- E. Gardner and B. Derrida. Optimal storage properties of neural network models. *Journal of Physics A Mathematical General*, 21:271–284, January 1988. doi: 10.1088/0305-4470/21/1/031.
- Andrey Gromov. Grokking modular arithmetic. *arXiv preprint arXiv:2301.02679*, 2023.
- Géza Györgyi. First-order transition to perfect generalization in a neural network with binary synapses. *Phys. Rev. A*, 41:7097–7100, Jun 1990. doi: 10.1103/PhysRevA.41.7097. URL <https://link.aps.org/doi/10.1103/PhysRevA.41.7097>.
- Lev Davidovich Landau and Evgenii Mikhailovich Lifshitz. *Statistical Physics: Volume 5*, volume 5. Elsevier, 2013.
- Qianyi Li and Haim Sompolinsky. Statistical mechanics of deep linear neural networks: The back-propagating kernel renormalization. *Phys. Rev. X*, 11:031059, Sep 2021. doi: 10.1103/PhysRevX.11.031059. URL <https://link.aps.org/doi/10.1103/PhysRevX.11.031059>.
- Ziming Liu, Ouail Kitouni, Niklas Nolte, Eric J Michaud, Max Tegmark, and Mike Williams. Towards understanding grokking: An effective theory of representation learning. In Alice H. Oh, Alekh Agarwal, Danielle Belgrave, and Kyunghyun Cho (eds.), *Advances in Neural Information Processing Systems*, 2022. URL <https://openreview.net/forum?id=6at6rB3IZm>.
- Song Mei, Andrea Montanari, and Phan-Minh Nguyen. A mean field view of the landscape of two-layer neural networks. *Proceedings of the National Academy of Sciences*, 115(33):E7665–E7671, 2018. ISSN 0027-8424. doi: 10.1073/pnas.1806579115. URL <https://www.pnas.org/content/115/33/E7665>.
- Beren Millidge. Grokking 'grokking'. 2022. URL <https://www.beren.io/2022-01-11-Grokking-Grokking/>.

- Neel Nanda, Lawrence Chan, Tom Lieberum, Jess Smith, and Jacob Steinhardt. Progress measures for grokking via mechanistic interpretability, 2023.
- Gadi Naveh, Oded Ben David, Haim Sompolinsky, and Zohar Ringel. Predicting the outputs of finite deep neural networks trained with noisy gradients. *Physical Review E*, 104(6), Dec 2021. ISSN 2470-0053. doi: 10.1103/physreve.104.064301. URL <http://dx.doi.org/10.1103/PhysRevE.104.064301>.
- Radford M Neal. Priors for infinite networks. In *Bayesian Learning for Neural Networks*, pp. 29–53. Springer, 1996.
- Radford M Neal et al. MCMC using hamiltonian dynamics. *Handbook of markov chain monte carlo*, 2(11):2, 2011.
- Roman Novak, Lechao Xiao, Jaehoon Lee, Yasaman Bahri, Greg Yang, Daniel A. Abolafia, Jeffrey Pennington, and Jascha Sohl-Dickstein. Bayesian Deep Convolutional Networks with Many Channels are Gaussian Processes. *arXiv e-prints*, art. arXiv:1810.05148, October 2018.
- Alethea Power, Yuri Burda, Harri Edwards, Igor Babuschkin, and Vedant Misra. Grokking: Generalization beyond overfitting on small algorithmic datasets. *arXiv preprint arXiv:2201.02177*, 2022.
- Carl Edward Rasmussen and Christopher K. I. Williams. *Gaussian Processes for Machine Learning (Adaptive Computation and Machine Learning)*. The MIT Press, 2005. ISBN 026218253X.
- David Saad and Sara A. Solla. Exact solution for on-line learning in multilayer neural networks. *Phys. Rev. Lett.*, 74:4337–4340, May 1995. doi: 10.1103/PhysRevLett.74.4337. URL <https://link.aps.org/doi/10.1103/PhysRevLett.74.4337>.
- Inbar Seroussi, Gadi Naveh, and Zohar Ringel. Separation of scales and a thermodynamic description of feature learning in some CNNs. *Nature Communications*, 14(1):908, 2023.
- H. S. Seung, H. Sompolinsky, and N. Tishby. Statistical mechanics of learning from examples. *Phys. Rev. A*, 45:6056–6091, Apr 1992. doi: 10.1103/PhysRevA.45.6056. URL <https://link.aps.org/doi/10.1103/PhysRevA.45.6056>.
- Naftali Tishby and Noga Zaslavsky. Deep learning and the information bottleneck principle, 2015.
- Bojan Žunkovič and Enej Ilievski. Grokking phase transitions in learning local rules with gradient descent. *arXiv e-prints*, art. arXiv:2210.15435, October 2022. doi: 10.48550/arXiv.2210.15435.
- Karl Weiss, Taghi M Khoshgoftaar, and DingDing Wang. A survey of transfer learning. *Journal of Big data*, 3(1):1–40, 2016.
- Christopher Williams. Computing with infinite networks. *Advances in neural information processing systems*, 9, 1996.
- Matthew D. Zeiler and Rob Fergus. Visualizing and understanding convolutional networks. In David Fleet, Tomas Pajdla, Bernt Schiele, and Tinne Tuytelaars (eds.), *Computer Vision – ECCV 2014*, pp. 818–833, Cham, 2014. Springer International Publishing. ISBN 978-3-319-10590-1.

SUPPLEMENTARY MATERIAL

A TEACHER-STUDENT MODEL

A.1 SCALING LIMIT OF TEACHER-STUDENT MODEL AND SAMPLE COMPLEXITY ASPECTS

Here we detail the scaling limits in which our results should become exact.

Our first requirement, is a mean-field scaling (χ) of the output layer weight, in the spirit of Refs. Mei et al. (2018); Bordelon & Pehlevan (2022). To this end, we define $\sigma_a^2 = \tilde{\sigma}_a^2/\chi$ (i.e. the microscopic variance of each readout layer weight is $\tilde{\sigma}_a^2/(\chi N)$ and $\sigma^2 = \tilde{\sigma}^2/\chi$). Notably, since $b, c \propto \sigma^2/[\sigma^2 + K]$ this has no effect on b or c . Examining the action, this yields an additional constant factor of χ in front of the non-linear term, as expected since mean-field scaling increases feature learning. Taking $\chi \gg 1$ controls the mean-field decoupling.

Our first *limit* is the continuum limit, where we take n to infinite, keeping $n/(\tilde{\sigma}^2) = n_{\text{eff}}$ fixed. This again does not change b, c nor the action of the weights as the latter contains only the combination $n/\tilde{\sigma}^2$. The resulting non-linear term in the action now appears as

$$\mathcal{S}[\mathbf{w}] = d \left(\frac{|\mathbf{w}|^2}{2\sigma_w^2} - \frac{2\chi n_{\text{eff}}^2 \tilde{\sigma}_a^2 (\mathbf{w} \cdot \mathbf{w}^*)^2}{\pi d N (1 + 2|\mathbf{w}|^2)} \left(b[n_{\text{eff}}/d] - \frac{2c[\epsilon] (\mathbf{w} \cdot \mathbf{w}^*)^2}{1 + 2|\mathbf{w}|^2} \right)^2 \right) \quad (1)$$

where we further indicated the dependencies of b and c which arise through GPR. Indeed, based on the equivalence kernel results discussed in the main text $b = (\tilde{\sigma}^2/n)/(\tilde{\sigma}^2/n + \tilde{\lambda})$ where $\tilde{\lambda} = O(1/d)$ whereas c due to its weak eigenvalue is fixed to ϵ (in principle it also depends on n_{eff}/d^3 which we neglect).

Our second limit is the ‘‘thermodynamic’’ limit, which helps justify the saddle point and hence allows for a well-defined phase transition. Here we take d to infinity while keeping a linear scaling between n_{eff}, N and d . This assures us that the action remains the same apart from the overall d factor. Changing χ or the linear scaling between d, n_{eff} and N all act as knobs controlling the phase transition.

We conjecture that the teacher-student model has a better sample complexity than the infinite-width network. Namely, the infinite-width network is able to learn the cubic target at, $n \propto d^3$ whereas the former can reach good accuracy at $n \propto d$. Replacing n with the above, n_{eff} the latter is implied by the linear scaling of and d, n_{eff} together with our analytical results, which show that the cubic component is being learned.

Establishing this more rigorously requires showing that n and n/σ^2 can be kept in the same order of d . Alternatively stated, that σ^2 may be large but does not need to scale as d . This can be potentially shown using corrections to EK derived in Ref. Cohen et al. (2019) where it is often sufficient to take just n large and not both n and σ^2 . We note by passing that even if χ , which divides σ^2 , has to scale as N (there increasing n/σ^2 compared to n) it would result in a scaling of $n \propto d^{1.5}$ which is still a notable improvement.

A.2 CONTINUUM ACTION AND MODE DECOUPLING

In the continuum limit, by substituting the sums appearing in eq. 6 of the main text for integrals, the action \mathcal{S} is given by-

$$\mathcal{S} = \frac{d|\mathbf{w}|^2}{2\sigma_w^2} - \frac{n^2 \sigma_a^2}{2N} \left[\int d\mu_{\mathbf{x}\bar{\mathbf{t}}}(\mathbf{x}) \phi(\mathbf{w} \cdot \mathbf{x}) \right]^2 \quad (2)$$

Using our self-consistent assumption about the discrepancy- $\bar{t}(\mathbf{x}) = bH_1(\mathbf{w}^* \cdot \mathbf{x}) + cH_3(\mathbf{w}^* \cdot \mathbf{x})$, we can compute the action in the continuum limit-

$$\begin{aligned} \mathcal{S} &\equiv \frac{d|\mathbf{w}|^2}{2\sigma_w^2} - \frac{n^2\sigma_a^2}{2N\sigma^4} \left(\underbrace{(b - 3c|\mathbf{w}^*|^2) \int d\mu_x(\mathbf{w}^* \cdot \mathbf{x}) \phi(\mathbf{w} \cdot \mathbf{x})}_{I_0} + c \underbrace{\int d\mu_x(\mathbf{w}^* \cdot \mathbf{x})^3 \phi(\mathbf{w} \cdot \mathbf{x})}_{I_1} \right)^2 \\ &= d \left(\frac{|\mathbf{w}|^2}{2\sigma_w^2} - \frac{2n^2\sigma_a^2}{\pi dN\sigma^4} \frac{(\mathbf{w} \cdot \mathbf{w}^*)^2}{1 + 2|\mathbf{w}|^2} \left(b - \frac{2c(\mathbf{w} \cdot \mathbf{w}^*)^2}{1 + 2|\mathbf{w}|^2} \right)^2 \right) \end{aligned} \quad (3)$$

we the integrals I_0, I_1 are computed in App. A.4.

In principle, one could perform saddle point analysis in two variables. A simplification can be made by noting that the dominant fluctuations are in the direction of \mathbf{w}^* . We are therefore projecting \mathbf{w} into the subspace of \mathbf{w}^* , such that, $\mathbf{w} = P_{\mathbf{w}^*}\mathbf{w} + P_{\mathbf{w}^*}^\perp\mathbf{w}$, with $P_{\mathbf{w}^*} = \frac{1}{|\mathbf{w}^*|^2}\mathbf{w}^*(\mathbf{w}^*)^T$, and $P_{\mathbf{w}^*}^\perp = I_d - P_{\mathbf{w}^*}$, Denote $\alpha = \mathbf{w}^* \cdot \mathbf{w}$ and $\alpha_\perp = |P_{\mathbf{w}^*}^\perp\mathbf{w}|$ the action is given by

$$\mathcal{S}[\mathbf{w}] = \frac{d}{2\sigma_w^2}\alpha^2 + \frac{d}{2\sigma_w^2}\alpha_\perp^2 - \frac{4n^2\sigma_a^2}{\pi 2N\sigma^4} \frac{|\mathbf{w}^*|^2\alpha^2}{1 + 2(\alpha^2 + \alpha_\perp^2)} \left(b - \frac{2c|\mathbf{w}^*|^2\alpha^2}{1 + 2(\alpha^2 + \alpha_\perp^2)} \right)^2, \quad (4)$$

By concentration of the norm, we replace α_\perp by its average σ_w^2 yields the action in the main text equation 14, which is an action only in one variable.

A.3 SOLVING THE EQUATIONS FOR b, c

Since the kernel does not mix polynomials of higher order, we can write the GPR expression for the mean network output in the function space spanned by the components of the target. Namely, any vector in this two-dimensional space, $\mathbf{v} = \begin{bmatrix} s \\ t \end{bmatrix}$ is given by

$$v(\mathbf{x}) = sH_1(\mathbf{w}^* \cdot \mathbf{x}) + \frac{t}{\sqrt{6}}H_3(\mathbf{w}^* \cdot \mathbf{x}) = s\hat{H}_1(\mathbf{x}) + t\hat{H}_3(\mathbf{x}) \quad (5)$$

The factor of $\frac{1}{\sqrt{6}}$ results from the requirement that the basis of this space will be normal. In this basis, the discrepancy and the target is given by,

$$\bar{\mathbf{t}} = \begin{bmatrix} b \\ \sqrt{6}c \end{bmatrix}, \mathbf{y} = \begin{bmatrix} 1 \\ \sqrt{6}\epsilon \end{bmatrix} \quad (6)$$

Note that here we denoted in bold $\bar{\mathbf{t}}$ the two dimensional vectors, and the discrepancy as a scalar can be thought of as

$$\bar{t} = \bar{\mathbf{t}} \cdot \begin{bmatrix} \hat{H}_1(\mathbf{x}) \\ \hat{H}_3(\mathbf{x}) \end{bmatrix} \quad (7)$$

And similarly for the target function. In this basis, the two dimensional kernel \tilde{Q} is given by

$$\hat{Q} = \begin{bmatrix} \int d\mu_x d\mu_z \hat{H}_1(\mathbf{x}) Q(\mathbf{x}, z) \hat{H}_1(z) & \int d\mu_x d\mu_z \hat{H}_3(\mathbf{x}) Q(\mathbf{x}, z) \hat{H}_1(z) \\ \int d\mu_x d\mu_z \hat{H}_1(\mathbf{x}) Q(\mathbf{x}, z) \hat{H}_3(z) & \int d\mu_x d\mu_z \hat{H}_3(\mathbf{x}) Q(\mathbf{x}, z) \hat{H}_3(z) \end{bmatrix} \quad (8)$$

where μ_x is the standard Gaussian measure, Q is the mean continuum limit kernel defined as

$$Q(\mathbf{x}, z) = \sigma_a^2 \int \frac{e^{-\mathcal{S}(\mathbf{w}; b, c)}}{\mathcal{Z}} \phi(\mathbf{x} \cdot \mathbf{w}) \phi(\mathbf{z} \cdot \mathbf{w}) d\mathbf{w} \quad (9)$$

Next, we proceed by calculating the matrix element of \hat{Q} . As shown in the integral appendix A.4, we have

$$\int d\mu_{\mathbf{x}} \hat{H}_1(\mathbf{x}) \phi(\mathbf{x} \cdot \mathbf{w}) = \frac{2(\mathbf{w}^* \cdot \mathbf{w})}{\sqrt{\pi} \sqrt{(1+2|\mathbf{w}|^2)}}$$

$$\int d\mu_{\mathbf{x}} \hat{H}_3(\mathbf{x}) \phi(\mathbf{x} \cdot \mathbf{w}) = -\frac{4(\mathbf{w}^* \cdot \mathbf{w})^3}{\sqrt{6\pi} \sqrt{(1+2|\mathbf{w}|^2)^3}}$$

Since the fluctuations in the directions orthogonal to \mathbf{w}^* are small, the quantity $|\mathbf{w}|^2$ appearing in the denominator can be approximated to $(\mathbf{w} \cdot \mathbf{w}^*)^2 + (d-1) \frac{\sigma_w^2}{d}$ as explained in the main text. Since we are taking large values of d , then $\frac{d-1}{d} \cong 1$. Additionally, we denote $\alpha = \mathbf{w} \cdot \mathbf{w}^*$, so that

$$\hat{Q} = \frac{\sigma_a^2}{\mathcal{Z}} \begin{bmatrix} \int \frac{2q^2 e^{-S(\alpha; b, c)}}{\pi(1+2(\alpha^2 + \sigma_w^2))} d\alpha & - \int \frac{8q^4 e^{-S(\alpha; b, c)}}{\sqrt{6\pi}(1+2(\alpha^2 + \sigma_w^2))^2} d\alpha \\ - \int \frac{8q^4 e^{-S(\alpha; b, c)}}{\sqrt{6\pi}(1+2(\alpha^2 + \sigma_w^2))^2} d\alpha & \int \frac{8q^6 e^{-S(\alpha; b, c)}}{3\pi(1+2(\alpha^2 + \sigma_w^2))^3} d\alpha \end{bmatrix}$$

Where $\mathcal{Z} = \int d\alpha e^{-S(\alpha; b, c)}$. These integrals are computed numerically, given, b, c to obtain self-consistent equations. Thus, \hat{Q} is a function of b, c , and on the other hand we can use \hat{Q} to obtain an expression for b, c through the GPR formula in this two-dimensional subspace,

$$\begin{bmatrix} b \\ \sqrt{6}c \end{bmatrix} = \bar{\mathbf{t}} = \left[\hat{Q} + \frac{\sigma^2}{n} I_2 \right]^{-1} \mathbf{y} = \left[\hat{Q} + \frac{\sigma^2}{n} I_2 \right]^{-1} \begin{bmatrix} 1 \\ \sqrt{6}\epsilon \end{bmatrix} \quad (10)$$

This results in two equations for b, c which can be solved numerically.

A.4 INTEGRAL CALCULATIONS FOR THE TEACHER-STUDENT MODEL

Here we compute the integral $\langle (\mathbf{w}^* \cdot \mathbf{x})^{2n+1} \phi(\mathbf{w} \cdot \mathbf{x}) \rangle_{\mathbf{x}}$ where $\mathbf{x} \sim \mathcal{N}(0, I_d)$. This integral appears both in the computation of the action and in the calculation of the matrix elements of \hat{Q} . Denote-

$$I_n \equiv \frac{1}{Z} \int d\mathbf{x} e^{-\frac{1}{2}\mathbf{x}^2} \phi(\mathbf{w} \cdot \mathbf{x}) (\mathbf{w}^* \cdot \mathbf{x})^{2n+1}. \quad (11)$$

Where $Z = (2\pi)^{d/2}$ is a normalizing factor. This integral is given by

$$\begin{aligned} I_n &\equiv \frac{1}{Z} \int d\mathbf{x} e^{-\frac{1}{2}\mathbf{x}^2} \phi(\mathbf{w} \cdot \mathbf{x}) (\mathbf{w}^* \cdot \mathbf{x})^{2n+1} \\ &= \frac{2}{\sqrt{\pi}} \frac{\mathbf{w} \cdot \mathbf{w}^*}{\sqrt{\det(\mathbf{1} + 2\mathbf{w}\mathbf{w}^T)}} \langle (\mathbf{w}^* \cdot \mathbf{x})^{2n} \rangle_{\mathcal{N}(0, (\mathbf{1} + 2\mathbf{w}\mathbf{w}^T)^{-1})} + 2n |\mathbf{w}^*|^2 I_{n-1} \\ &= \frac{2}{\sqrt{\pi}} \frac{\mathbf{w} \cdot \mathbf{w}^*}{\sqrt{1+2|\mathbf{w}|^2}} \langle (\mathbf{w}^* \cdot \mathbf{x})^{2n} \rangle_{\mathcal{N}(0, (\mathbf{1} + 2\mathbf{w}\mathbf{w}^T)^{-1})} + 2n |\mathbf{w}^*|^2 I_{n-1} \end{aligned} \quad (12)$$

By Sherman Morrison's formula,

$$(\mathbf{1} + 2\mathbf{w}\mathbf{w}^T)^{-1} = \mathbf{1} - \frac{2\mathbf{w}\mathbf{w}^T}{1+2|\mathbf{w}|^2}. \quad (13)$$

Therefore, a recursive expression for I_n can be obtained in terms of \mathbf{w} and I_{n-1}

$$\begin{aligned} I_n &= \frac{1}{Z} \int d\mathbf{x} e^{-\frac{1}{2}\mathbf{x}^2} \phi(\mathbf{w} \cdot \mathbf{x}) (\mathbf{w}^* \cdot \mathbf{x})^{2n+1} \\ &= \frac{2}{\sqrt{\pi}} \frac{\mathbf{w} \cdot \mathbf{w}^*}{\sqrt{1+2|\mathbf{w}|^2}} \langle (\mathbf{w}^* \cdot \mathbf{x})^{2n} \rangle_{\mathcal{N}(0, (\mathbf{1} + 2\mathbf{w}\mathbf{w}^T)^{-1})} + 2n |\mathbf{w}^*|^2 I_{n-1}. \end{aligned} \quad (14)$$

The cases $n = 0, 1$ are the ones used in this work. For $n = 0$ the integral is simply-

$$I_0 = \frac{2}{\sqrt{\pi}} \frac{\mathbf{w} \cdot \mathbf{w}^*}{\sqrt{1 + 2|\mathbf{w}|^2}}. \quad (15)$$

For $n = 1$ the calculation is slightly more complicated. We have

$$\begin{aligned} \langle (\mathbf{w}^* \cdot \mathbf{x})^2 \rangle &= \sum_{ij} w'_i w'_j \langle x_i x_j \rangle = \sum_{ij} w'_i w'_j \left[(\mathbf{1} + 2\mathbf{w}\mathbf{w}^T)^{-1} \right]_{ij} \\ &= \sum_{ij} w'_i w'_j \left[\delta_{ij} - \frac{2w_i w_j}{1 + 2|\mathbf{w}|^2} \right] \\ &= |\mathbf{w}^*|^2 - \frac{2(\mathbf{w} \cdot \mathbf{w}^*)^2}{1 + 2|\mathbf{w}|^2}. \end{aligned} \quad (16)$$

Which yield,

$$I_1 = \frac{2}{\sqrt{\pi}} \frac{(\mathbf{w} \cdot \mathbf{w}^*)}{\sqrt{(1 + 2|\mathbf{w}|^2)}} \left(3|\mathbf{w}^*|^2 - \frac{2(\mathbf{w} \cdot \mathbf{w}^*)^2}{1 + 2|\mathbf{w}|^2} \right) \quad (17)$$

B MODULAR ALGEBRA

B.1 MODULAR ALGEBRA KERNEL AND SYMMETRIES

We are first concerned with the spectral properties of $Q_{nm, n'm'}$, the latter being the average of $\tilde{Q}_{nm, n'm'}$ with respect $S[\mathbf{w}]$. To this end note some useful model symmetries that occur when n_{train} spans the entire training set. By symmetries here we mean that the training algorithm, neural network, and the data-set are invariant remain invariant under the following transformations:

- I. Taking $[n, m] \rightarrow [(n + q) \bmod P, (m + q') \bmod P]$, and $f_p \rightarrow f_{(p+q+q') \bmod P}$ with $q, q' \in \mathbb{Z}_P$
- II. Taking $[n, m] \rightarrow [qn \bmod P, qm \bmod P]$ and $f_p \rightarrow f_{qp \bmod P}$ for $q \in \mathbb{Z}_P$ but different than zero.

Notably, Q does not contain any reference to a specific label (p). Hence, both these symmetries are symmetries of Q (both before and after any potential phase transition). Specifically, let us denote by T_1 (T_2) the orthogonal transformation taking $[n, m] \rightarrow [n + 1, m] \bmod P$ ($[n, m] \rightarrow [n, m + 1] \bmod P$) and by C_q the transformation taking $[n, m] \rightarrow [qn, qm] \bmod P$. Then the following commutation relations holds,

$$\begin{aligned} [Q, T_1] &= [Q, T_2] = [Q, C_q] = 0 \\ [T_1, T_2] &= 0 \end{aligned} \quad (18)$$

This implies that Q, T_1 and T_2 can be diagonalized on the same basis. The Fourier basis $(\phi_{k, k'})$, discussed in the main text, clearly diagonalizes T_1 and T_2 simultaneously. Furthermore, as no two $\phi_{k, k'}$ share the same eigenvalues of T_1 and T_2 , each $\phi_{k, k'}$ must be an eigenfunction of Q .

Next, we notice that since $[Q, C_q] = 0$, $C_q \phi_{k, k'}$ must also be an eigenvector of Q with the same eigenvalue. However, since $[T_{1,2}, C_q] \neq 0$ C_q shifts us between, $\phi_{k, k'}$ hence implying degenerates. Based on the definition of the Fourier modes, we find $C_q \phi_{k, k'} = \phi_{qk, qk'}$ hence all pairs of momentum (k, k', g, g') such that $k = qg, k' = qg'$ must have degenerate eigenvalues. Notably for prime P for any $k, g \neq 0$ there exists a q such that $qk = g$. We furthermore note that an additional ‘‘flip’’ symmetry exists, implying that k, k' are associated with the same eigenvalue as k', k .

The above results for Q hold exactly regardless of network width, noise, or other hyperparameters. Next, we focus on Q at the NNGP limit ($N \rightarrow \infty$), which according to our saddle-point treatment, is also the kernel at any point before the phase transition (at large P). Here we find an enhanced

symmetry which explains its poor performance. Indeed, before the phase transition, The kernel Q is given

$$\begin{aligned} Q_{nm,n'm'} &= \sigma_a^2 [K_{nm,nm}K_{n'm',n'm'} + 2K_{nm,n'm'}^2] \\ K_{nm,n'm'} &= \langle (W_n + W_{m+P})(W_{n'} + W_{m'+P}) \rangle_{\mathbf{w} \sim N[0, I_{2P \times 2P}]} \\ &= \delta_{n,n'} + \delta_{m+P,m'+P} + \delta_{n,m'+P} + \delta_{m+P,n'} \\ &= \delta_{n,n'} + \delta_{m,m'} \end{aligned} \quad (19)$$

where we recall that $n, m \in [0..P-1]$. Given that, one can act with symmetry II separately on each index. This extra symmetry implies, via the above arguments, that all k, k' , and q, q' with $k = ck'$ and $q = c'q'$ are equivalent. For prime, P this results in only 3 distinct eigenvalues - the one associated with $k, k' = 0, 0$, the one associated with all 0, $k \neq 0$ and $k \neq 0, 0$ modes and the one (λ) associated with $k \neq 0, k' \neq 0$. Notably, the target is supported only on this last $(P-1)^2$ -dimensional degenerate subspace. The equal prior on $(P-1)^2$ eigenfunctions then implies $O(P^2)$ examples are needed for the GP to perform well on the task here, namely the entire multiplication table.

B.2 FOURIER TRANSFORM OF THE ACTION

Here we compute the action in Fourier space without the weight decay term which appears in the main text. To construct the Fourier transformed action, we start from the fluctuating kernel term (\tilde{Q}) given by

$$\sigma_a^{-2} \tilde{Q} = \sum_{n,n'=0}^P \sum_{m,m'=P}^{2P-1} (w_m + w_n)^2 (w_{m'} + w_{n'})^2 |n, m\rangle \langle n', m'| \quad (20)$$

where we have used physics-style bra-ket notation to denote the basis on which the operator \tilde{Q} is presented. For instance, $\tilde{Q}_{n_0 m_0, n'_0 m'_0}$ is given by acting with $\langle n_0, m_0 |$ from the left and $|n'_0, m'_0\rangle$ from the right and using $\langle n_0, m_0 | n_1, m_1 \rangle = \delta_{n_0, n_1} \delta_{m_0, m_1}$.

Based on the symmetries of the problem we consider the following coordinate transformation

$$w_m \mapsto \sum_{k=0}^{P-1} w_k e^{-\frac{2\pi i}{P} kn}, \quad w_n \mapsto \sum_{k=0}^{P-1} v_k e^{-\frac{2\pi i}{P} km} \quad (21)$$

Substituting this in the equation for \tilde{Q} :

$$\begin{aligned} \tilde{Q} &= \sum_{kk'qq'} \sum_{m,n} \underbrace{\left(w_k e^{-\frac{2\pi i}{P} kn} + v_k e^{-\frac{2\pi i}{P} km} \right) \left(w_{k'} e^{-\frac{2\pi i}{P} k'n} + v_{k'} e^{-\frac{2\pi i}{P} k'm} \right)}_J |n, m\rangle \\ &\quad \cdot \underbrace{\left(w_q e^{\frac{2\pi i}{P} qn'} + v_q e^{\frac{2\pi i}{P} qm'} \right) \left(w_{q'} e^{\frac{2\pi i}{P} q'n'} + v_{q'} e^{\frac{2\pi i}{P} q'm'} \right)}_{J'} \langle n', m'| \end{aligned} \quad (22)$$

Where we can simplify further

$$J = \sum_{mn} \left(w_k w_{k'} e^{-\frac{2\pi i}{P} (k+k')n} + v_k v_{k'} e^{-\frac{2\pi i}{P} (k+k')m} + w_{k'} v_k e^{-\frac{2\pi i}{P} (k'n+km)} + w_k v_{k'} e^{-\frac{2\pi i}{P} (kn+k'm)} \right) |n, m\rangle \quad (23)$$

$$\equiv P (w_k w_{k'} |k+k', 0\rangle + v_k v_{k'} |0, k+k'\rangle + w_k v_{k'} |k, k'\rangle + w_{k'} v_k |k', k\rangle),$$

(which also serves as the definition of the Fourier transformed bra-ket notation) and similarly for the conjugated term:

$$J' = P (\langle -q, -q' | w_q v_{q'} + \langle -q', -q | w_{q'} v_q + \langle -(q+q'), 0 | w_q w_{q'} + \langle 0, -(q+q') | v_q v_{q'}) \quad (24)$$

We next turn to the quadratic term

$$\begin{aligned} \sum_{n=0}^{P-1} w_n^2 &= \sum_{n=0}^{P-1} \sum_{k,k'=0}^{P-1} w_k w_{k'} e^{\frac{2\pi i}{P}(k+k')n} \\ &= P \sum_{k=0}^{P-1} w_k w_{-k}, \end{aligned} \quad (25)$$

using $\sum_{n=0}^{P-1} e^{\frac{2\pi i}{P}(k+k')n} = P\delta_{k,-k}$. The quadratic term in the action (main text equation 15) $|\mathbf{w}|^2$ is given by

$$|\mathbf{w}|^2 = \sum_{n=0}^{P-1} w_n^2 + \sum_{m=P}^{2P-1} w_m^2 = P \left(\sum_{k=0}^{P-1} w_k w_{-k} + \sum_{k=0}^{P-1} v_k v_{-k} \right) \quad (26)$$

The target can be also expressed in terms of the Fourier basis, noting that the mode zero is zero for P prime

$$y_{nm}^p = P^{-1} \sum_{k=1}^{P-1} e^{-i2\pi kp/P} e^{i2\pi k(n+m)/P} = \langle n, m | \sum_{q=1}^{P-1} e^{-2\pi i q p/P} |q, q\rangle \quad (27)$$

The remaining term in the action (main text equation 21) following the anzats $t = ay$, and considering the whole dataset. the involves the kernel and is given by

$$\begin{aligned} &\sum_{p,mn,m'n'} y_{nm}^p \bar{y}_{n'm'}^p \tilde{Q}_{nmn'm'} \\ &= \sum_{p,mn,m'n'} \langle n, m | \sum_{q=1}^{P-1} e^{-2\pi i q p/P} |q, q\rangle \langle n', m' | \sum_{q'} e^{2\pi i q' p/P} |q', q'\rangle \tilde{Q}_{nmn'm'} \\ &= \sum_{mn,m'n'} \sum_{q,q'=1}^{P-1} \langle n, m | q, q\rangle \langle n', m' | q', q'\rangle \tilde{Q}_{nn'mm'} \sum_p e^{-2\pi i (q'-q)p/P} \\ &= P \sum_{mn,m'n'} \sum_{q,q'} \langle n, m | q, q\rangle \langle n', m' | q', q'\rangle \tilde{Q}_{nn'mm'} \delta_{q,q'} \\ &= P \sum_q \langle q, q | \left[\sum_{mn,m'n'} \tilde{Q}_{nn'mm'} |n, m\rangle \langle n', m'| \right] |q, q\rangle \\ &= P \sum_{q=1}^{P-1} \langle q, q | \tilde{Q} |q, q\rangle \end{aligned} \quad (28)$$

Note that the chosen basis is orthonormal, so that $\langle t | k\rangle = \delta_{k,t}$ and thus all terms with $|0\rangle$ vanish and, and we are left with-

$$\begin{aligned} &P \sum_{t=1}^{P-1} \langle t, t | \tilde{Q} |t, t\rangle \\ &= P^3 \sum_{kk'qq'} \sum_{t=1}^{P-1} \langle t, t | (w_k v_{k'} |k, k'\rangle + w_{k'} v_k |k', k\rangle) (w_q v_{q'} \langle -q, -q'| + w_{q'} v_q \langle -q', -q|) |t, t\rangle \\ &= P^3 \sum_{kk'qq'} \sum_{t=1}^{P-1} (w_k v_{k'} \delta_{k,t} \delta_{k',t} + w_{k'} v_k \delta_{k,t} \delta_{k',t}) (w_q v_{q'} \delta_{-q,t} \delta_{-q',t} + w_{q'} v_q \delta_{-q,t} \delta_{-q',t}) \\ &= 4P^3 \sum_{t=1}^{P-1} w_t v_t w_{-t} v_{-t}. \end{aligned} \quad (29)$$

The action in Fourier space is then given by

$$\mathcal{S}[\hat{w}] = P \left[\left(\frac{1}{2} \sum_{k=0}^{P-1} w_k w_{-k} + \frac{1}{2} \sum_{k=0}^{P-1} v_k v_{-k} \right) - \frac{2\sigma_a^2 a^2 P^2}{N\sigma^4} \sum_{k=1}^{P-1} w_k w_{-k} v_k v_{-k} \right]. \quad (30)$$

Note that since the weights are all real, the Fourier transforms obey $\overline{w_k} = w_{-k}$, we can therefore rewrite \mathcal{S} in terms of the parameters $|w_k|, |v_k|$

$$\mathcal{S}[\hat{w}] = P \left[\frac{1}{2} \sum_{k=0}^{P-1} (|w_k|^2 + |v_k|^2) - \frac{2\sigma_a^2 a^2 P^2}{N\sigma^4} \sum_{k=1}^{P-1} |w_k|^2 |v_k|^2 \right]. \quad (31)$$

So that the action can be separated into independent actions \mathcal{S}_k that each depend on different values of k

$$\begin{aligned} \mathcal{S}[\hat{w}] &= \sum_{k \neq 0}^{P-1} P \left[\frac{1}{2} (|w_k|^2 + |v_k|^2) - \frac{2\sigma_a^2 a^2 P^2}{N\sigma^4} |w_k|^2 |v_k|^2 \right] + \frac{1}{2} (|w_0|^2 + |v_0|^2) \\ &\equiv \mathcal{S}_0(|w_0|, |v_0|) + \sum_{k \neq 0}^{P-1} \mathcal{S}_k(|w_k|, |v_k|) \end{aligned} \quad (32)$$

B.3 SOLVING THE EQUATION FOR a

As done in the teacher-student model, obtaining a self-consistent equation for the discrepancy requires averaging the kernel with respect to the weights. Here, \tilde{Q} is given by-

$$\begin{aligned} \tilde{Q} &= \sum_{k, k', q, q'} (w_k w_{k'} |k + k', 0\rangle + v_k v_{k'} |0, k + k'\rangle + w_k v_{k'} |k, k'\rangle + w_{k'} v_k |k', k\rangle) \cdot \\ &\cdot (\langle -q, -q' | w_q v_{q'} + \langle -q', -q | w_{q'} v_q + \langle -(q + q'), 0 | w_q w_{q'} + \langle 0, -(q + q') | v_q v_{q'} \rangle \end{aligned} \quad (33)$$

Since the action in Fourier space depends only on the magnitude of the weights and not on the phase, we deduce that the phases are uniformly distributed on the unit circle and are independent of the magnitudes. There are multiple types of terms that appear in \tilde{Q} , and we will calculate each part individually:

1. For terms of the form- $w_k v_{k'} w_q v_{q'}$, we have- $\langle w_k v_{k'} w_q v_{q'} \rangle = \langle |w_k| |v_{k'}| |w_q| |v_{q'}| \rangle \langle e^{i(\phi_k + \phi_{k'} + \theta_{k'} + \theta_{q'})} \rangle$. Since the phases of v, w are independent, then $\langle e^{i(\phi_k + \phi_{k'} + \theta_{k'} + \theta_{q'})} \rangle = \langle e^{i(\phi_k + \phi_{k'})} \rangle \langle e^{i(\theta_{k'} + \theta_{q'})} \rangle$. If $q \neq \pm k$ then $\langle e^{i(\phi_k + \phi_{k'})} \rangle = \langle e^{i\phi_k} \rangle \langle e^{i\phi_{k'}} \rangle$ and since the phases are uniformly distributed over $[0, 2\pi]$ these averages vanish and if $q = k$ then $\langle e^{i(\phi_k + \phi_{k'})} \rangle = \langle e^{2i\phi_k} \rangle$ which vanishes too, so that $\langle e^{i(\phi_k + \phi_{k'})} \rangle = \delta_{k, -k}$. Similarly, $\langle e^{i(\theta_{k'} + \theta_{q'})} \rangle = \delta_{k', -q'}$. Thus, we have- $\langle w_k v_{k'} w_q v_{q'} \rangle = \delta_{k', -q'} \delta_{k, -q} \langle |w_k|^2 |v_{k'}|^2 \rangle$
2. For terms such as- $\langle w_k w_{k'} w_q v_{q'} \rangle$, by averaging over the phases of $v_{q'}$ the term vanishes, and similarly terms like $\langle w_k v_{k'} v_q v_{q'} \rangle$ vanish.
3. We are left with terms of the form- $\langle w_k w_{k'} w_q w_{q'} \rangle$, for this not to vanish, we require $\phi_k + \phi_{k'} + \phi_q + \phi_{q'} = 0$ so that either $k = -k'$ and $q = -q'$, $k = -q$ and $k' = -q'$ or $k = -q', k' = -q$. The same is true for $\langle v_k v_{k'} v_q v_{q'} \rangle$.

In conclusion, the average kernel is given by-

$$\begin{aligned}\sigma_a^{-2}Q &= \sum_{k,k'=0}^{P-1} \left\langle |w_k|^2 |v_{k'}|^2 \right\rangle |k, k'\rangle \langle k, k'| \\ &+ \sum_{k,k'=0}^{P-1} \left\langle |w_k|^2 |w_{k'}|^2 \right\rangle (2|k+k', 0\rangle \langle k+k', 0| + |0, 0\rangle \langle 0, 0|) \\ &+ \sum_{k,k'=0}^{P-1} \left\langle |v_k|^2 |v_{k'}|^2 \right\rangle (2|0, k+k'\rangle \langle 0, k+k'| + |0, 0\rangle \langle 0, 0|)\end{aligned}\quad (34)$$

Since the target has no $|0\rangle$ component, it is orthogonal to the vectors $\langle k+k', 0|$, $\langle 0, k+k'|$ and $\langle 0, 0|$ so that these terms don't contribute when Q acts on the target. We are left with-

$$\begin{aligned}\sigma_a^{-2}Q\mathbf{y}^P &= \sum_{t=1}^{P-1} e^{\frac{2\pi i}{P}pt} Q|t, t\rangle = \sum_{t=1}^{P-1} e^{\frac{2\pi i}{P}pt} \sum_{k,k'=0}^{P-1} \left\langle |w_k|^2 |v_{k'}|^2 \right\rangle |k, k'\rangle \delta_{t,k} \delta_{t,k'} \\ &= \sum_{k=1}^{P-1} e^{\frac{2\pi i}{P}pk} \left\langle |w_k|^2 |v_k|^2 \right\rangle |k, k\rangle = \sigma_a^{-2} \lambda \mathbf{y}^P\end{aligned}\quad (35)$$

Since for all $k \neq 0$ the actions are identical, the mean

$$\lambda = \sigma_a^2 \left\langle |w_k|^2 |v_k|^2 \right\rangle = \sigma_a^2 \frac{\int \left(|w_k|^2 |v_k|^2 \right) e^{-S_k(|w_k|, |v_k|; a)}}{\int e^{-S_k(|w_k|, |v_k|; a)}},$$

is a constant function of a for every k . Thus, it can be deduced that the target in an eigenvector of Q , with an eigenvalue λ . A self-consistent equation for a is obtained using the GPR formula, where-

$$a = -\frac{\sigma^2}{\lambda(a) + \sigma^2}\quad (36)$$

B.4 CALCULATING THE EIGENVALUE OF THE TARGET

In the limit of $P \gg 1$, the quantity $\left\langle |w_k|^2 |v_k|^2 \right\rangle$ can be estimated using a saddle point approximation. The minimum of the action can be found by minimizing with respect to $|w_k|, |v_k|$ -

$$\begin{aligned}0 &= |w_k| - \frac{8\sigma_a^2 a^2 P}{N} |w_k| |v_k|^2 + \epsilon |w_k|^5 \\ &= |w_k| \left(1 - \frac{8\sigma_a^2 a^2 P}{N} |v_k|^2 + \epsilon |w_k|^4 \right)\end{aligned}\quad (37)$$

$$\begin{aligned}0 &= |v_k| - \frac{8\sigma_a^2 a^2 P}{N} |w_k|^2 |v_k| + \epsilon |v_k|^5 \\ &= |v_k| \left(1 - \frac{8\sigma_a^2 a^2 P}{N} |w_k|^2 + \epsilon |v_k|^4 \right)\end{aligned}\quad (38)$$

If $|w_k|, |v_k|$ are both nonzero, then from symmetry we assume that $|w_k|^2 = |v_k|^2$, so that

$$|v_k|^2 = |w_k|^2 = \frac{1}{\gamma} \left(\frac{2\sigma_a^2 a^2 P^2}{N} \pm \sqrt{\left(\frac{2\sigma_a^2 a^2 P^2}{N} \right)^2 - \gamma} \right) := w_{\pm}^2$$

If $|w_k| = 0$ then either $|v_k| = 0$ or $(-\gamma)^{-\frac{1}{4}}$, but since we chose a positive γ this is not possible. Similarly choosing $|v_k| = 0$ results in $|w_k| = 0$ so that either both are zero, or we have- $|v_k|^2 = |w_k|^2 = w_{\pm}^2$. Using saddle point approximation, we have for $k \neq 0$

$$P(|w_k|, |v_k|) = \frac{4e^{-S_k(w_+, w_+)} \delta(|w_k| - w_+) \delta(|v_k| - w_+) + \delta(|w_k|) \delta(|v_k|)}{1 + e^{-S_k(w_+, w_+)}}\quad (39)$$

In principle the leading order fluctuations near zero should appear in the probability distribution. However, this term can be discarded since the fluctuations in w_k, v_k are of order P^{-1} and so this contributes to λ terms of order P^{-2} so these are higher order corrections and can be ignored. With this discrete probability distribution, the matrix elements of Q can be computed as follows

$$\langle |w_k|^2 |v_k|^2 \rangle = \frac{w_+^4 e^{-S_k(w_+, w_+)}}{1 + e^{-S_k(w_+, w_+)}} \quad (40)$$

C EXPERIMENTAL SETUP

Networks were trained for 120000 epochs, with lr $2 \cdot 10^{-3}$ with varying noise and targets as detailed in the graphs. The networks were trained on ten different randomly generated datasets, with at least five different networks trained on each dataset. Parameters of the networks in all cases were $N = 700, n = 6000, d = 150, \sigma_w^2 = 0.5, \sigma_a^2 = 8$ error bars were calculated by dividing up the sets of trained networks into 5 subsets with 10-15 (depending on the exact set of training parameters) networks each. The histogram of the weights in the w^* direction were calculated in each network separately, and the value of the action in a certain bin was given by the average over these ensembles. The error was obtained by dividing the std by the square root of the number of samples per ensemble. In the calculation for the average network output, the value for b, c was computed as an average over the different datasets, and the error is given by the std.